



Fabrication of well-shaped $\text{Sr}_2\text{KTa}_5\text{O}_{15}$ nanorods with a tetragonal tungsten bronze structure by a flux method for artificial photosynthesis

Zeai Huang ^a, Kentaro Teramura ^{a,b,*}, Saburo Hosokawa ^{a,b}, Tsunehiro Tanaka ^{a,b,*}

^a Department of Molecular Engineering, Graduate School of Engineering, Kyoto University, Kyoto 615-8510, Japan

^b Elements Strategy Initiative for Catalysts and Batteries, Kyoto University, Kyoto 615-8510, Japan

ARTICLE INFO

Article history:

Received 20 May 2016

Received in revised form 13 June 2016

Accepted 18 June 2016

Available online 18 June 2016

Keywords:

Photocatalyst

CO_2 reduction

Evolution of O_2

Flux method

TTB structure

ABSTRACT

$\text{Sr}_2\text{KTa}_5\text{O}_{15}$ nanorods with a tetragonal tungsten bronze structure were synthesized by a facile one-pot method using potassium chloride (KCl) as flux. Only the flux method obtained pure nanorods under the same calcination temperature and time comparing with that of solid-state reaction (SSR) and polymerized complex (PC) methods. The as-fabricated $\text{Sr}_2\text{KTa}_5\text{O}_{15}$ nanorods with a Ag cocatalyst showed relatively high activity and good selectivity toward CO evolution in the photocatalytic conversion of CO_2 by H_2O . Stoichiometric amounts of O_2 as an oxidation product together with those of CO and H_2 as reduction products were obtained, indicating that H_2O worked as an electron donor in the photocatalytic conversion of CO_2 . The $\text{Sr}_2\text{KTa}_5\text{O}_{15}$ nanorods fabricated at 1173 K for 3 h in the mass ratio of KCl flux to precursors at 1.0 afforded the highest formation rate of CO evolution ($65.5 \mu\text{mol h}^{-1}$) and good selectivity toward CO evolution (88.7%).

© 2016 Elsevier B.V. All rights reserved.

1. Introduction

Despite limited natural resources of fossil fuels, energy consumption has increased dramatically in recent times, resulting in increased CO_2 emissions, which leads to global warming and climate change [1]. Finding a solution to the energy consumption problem and global warming is, therefore, a matter of urgency. For this, it is important to reduce the amount of CO_2 emissions from fossil fuels, because CO_2 is a major greenhouse gas. Solar energy conversion has been gaining attention as a promising new-generation energy production system for energy development. The primary goal of researchers in this field is to capture, convert, and store solar energy for later use. One way to address these challenges is to convert CO_2 into valuable products such as fuels and chemical feedstock using sunlight in the near future [2]. The conversion of CO_2 using a heterogeneous photocatalyst is one of the most promising methods of obtaining other carbon sources such as carbon monoxide (CO), formic acid (HCOOH), formaldehyde (HCHO), methanol (CH_3OH), and methane (CH_4) [3–5]. Moreover, the photo-

catalytic conversion of CO_2 using H_2O as an electron donor is considered to be one of the best methods to derive these carbon sources from CO_2 , while simultaneously carrying out water redox reaction to obtain H_2 and O_2 [6].

Since the 1970s when several research groups demonstrated photoelectrocatalytic reduction of CO_2 by H_2O to carbon sources such as HCHO and CH_3OH , the interest in this field has increased dramatically [7,8]. Until now, many studies have reported the use of various heterogeneous catalysts for the photocatalytic conversion of CO_2 by H_2O [9–11]. However, the main product, in most cases, is H_2 rather than carbon sources [12,13]. This is because formation of H_2 is a more preferred process compared to the reduction of CO_2 , since it is easier to reduce H_2O to H_2 ($E^0 = -0.41 \text{ V}$ at $\text{pH} = 7$ vs. NHE) than to reduce CO_2 to even the simplest CO carbon source ($E^0 = -0.52 \text{ V}$ at $\text{pH} = 7$ vs. NHE) [14,15]. In contrast to the reduction of H^+ , the photogenerated electron has to be consumed to reduce CO_2 ; therefore, it is very important to check the selectivity of the generated electrons for the reduction products of CO_2 such as CO, HCOOH, HCHO, CH_3OH , and CH_4 .

Our group has previously reported that ZnGa_2O_4 -modified Ga_2O_3 [16], ZnGa_2O_4 [17], $\text{La}_2\text{Ti}_2\text{O}_7$ [18], and SrO -modified Ta_2O_5 [19], with a Ag cocatalyst, which have shown relatively high activity for the photocatalytic conversion of CO_2 to CO as a primary reduction product by H_2O . It is well known that the Ag cocatalyst exhibits good selectivity toward CO evolution for the photocat-

* Corresponding authors at: Department of Molecular Engineering, Graduate School of Engineering, Kyoto University, Kyoto 615-8510, Japan.

E-mail addresses: teramura@moleng.kyoto-u.ac.jp (K. Teramura), tanakat@moleng.kyoto-u.ac.jp (T. Tanaka).

alytic conversion of CO_2 by H_2O [20,21]. A stoichiometric amount of O_2 as the oxidation product was obtained, indicating that H_2O , as an electron donor, is oxidized by four holes during the photocatalytic conversion of CO_2 . More importantly, Ag as the cocatalyst not only enhances the photocatalytic activity but also increases the selectivity toward CO evolution in an aqueous solution of NaHCO_3 . However, only a few studies have investigated materials that exhibit both high photocatalytic activity and good selectivity toward the desired reduction products in photocatalytic conversion of CO_2 .

Very recently, Kudo and co-workers reported that $\text{KCaSrTa}_5\text{O}_{15}$ with a tetragonal tungsten bronze (TTB) structure synthesized by a SSR method shows activity for the photocatalytic conversion of CO_2 by H_2O [22]. The synthesized $\text{KCaSrTa}_5\text{O}_{15}$ showed irregular morphology, resulting in limited reduction of CO_2 by H_2O and preferential occurrence of water splitting. $\text{KCaSrTa}_5\text{O}_{15}$ fabricated by a PC method showed approximately 90% selectivity toward CO evolution in the photocatalytic conversion of CO_2 by H_2O due to well-crystallized particles [23]. High calcination temperature or/and complicated fabrication process are necessary in the SSR and PC methods. Nevertheless, these reports suggest that the number of active sites available on the catalyst surface for the reduction of CO_2 and H^+ might be depend on the morphology, resulting in the change of the selectivity toward CO evolution in the photocatalytic conversion of CO_2 by H_2O . As described above, our study aims to fabricate catalysts for the photocatalytic conversion of CO_2 by H_2O with good activity and selectivity toward desired reduction products.

In this study, we modified a flux method to synthesize $\text{Sr}_2\text{KTa}_5\text{O}_{15}$ nanorods with the TTB structure to achieve high photocatalytic activity and good selectivity toward CO evolution after loading a Ag cocatalyst. Comparing with SSR and PC methods, the flux method not only obtained the pure phase of $\text{Sr}_2\text{KTa}_5\text{O}_{15}$ with regular morphology in a low calcination temperature and a short calcination time, but also showed high photocatalytic activity and good selectivity toward CO evolution. It was found that the photocatalytic activity for CO_2 conversion by H_2O was significantly affected by the preparation methods, calcination temperature, calcination time, and amount of flux.

2. Experimental

2.1. Fabrication of $\text{Sr}_2\text{KTa}_5\text{O}_{15}$ and deposition of cocatalyst

$\text{Sr}_2\text{KTa}_5\text{O}_{15}$ was fabricated by a KCl flux method with modification of the reported literature by Wark et al. [24]. A stoichiometric mixture of K_2CO_3 (99.5%, Wako), SrCO_3 (99.9%, Wako), and Ta_2O_5 (99.9%, Kojundo) was ground with a specific amount of KCl (99.9%, Wako) in an Al_2O_3 crucible for 5 min. The mass ratio of the KCl used as flux to the precursors (K_2CO_3 , SrCO_3 , and Ta_2O_5) is abbreviated as F/P (flux/precursors). The mixture mentioned above was then transferred to a 50 mL the Al_2O_3 crucible. The resulting mixture was calcined from 1123 K to 1373 K for 1–20 h in air. After cooling down to room temperature, the mixture was thoroughly washed with 300 mL distilled water at 358 K and then filtered with 1.0 L hot water in order to remove any residual salts, and then dried in air at 80 °C.

The Ag cocatalyst was deposited to the as-fabricated $\text{Sr}_2\text{KTa}_5\text{O}_{15}$ by a chemical reduction method. Specifically, 1.8 mL of an aqueous NaPH_2O_2 solution (0.33 mol L⁻¹) was added to 50 mL of a suspension of the photocatalyst (1.5 g) containing 1.4 mL of AgNO_3 (0.1 mol L⁻¹). After stirring at 358 K for 1.5 h, the suspension was filtered and dried in air at room temperature for further use.

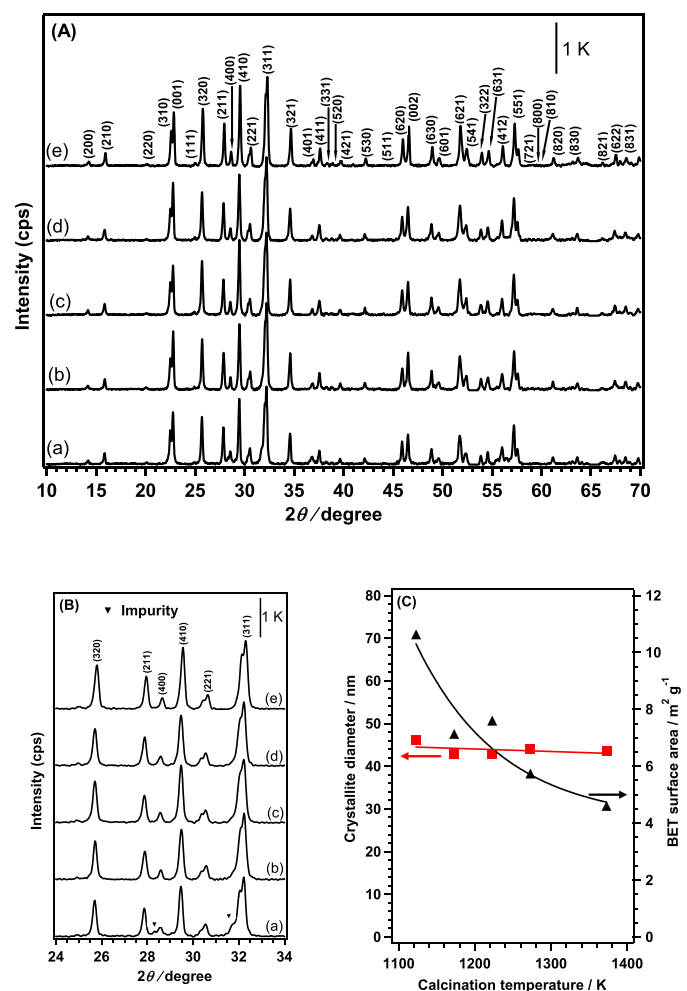


Fig. 1. (A) XRD patterns of $\text{Sr}_2\text{KTa}_5\text{O}_{15}$ calcined at 1123 K (a), 1173 K (b), 1223 K (c), 1273 K (d), and 1373 K (e) for 3 h in KCl flux ($\text{F}/\text{P} = 2.0$); (B) The enlarged XRD patterns of the above samples at the 2θ range from 24° to 34°; (C) Crystallite diameter of the (320) plane and BET specific surface area of $\text{Sr}_2\text{KTa}_5\text{O}_{15}$ prepared at different calcination temperatures.

2.2. Characterization

The structure and crystallinity of the samples were characterized by X-ray diffraction (XRD) using a Rigaku Multiflex powder X-ray diffractometer. The Brunauer–Emmett–Teller (BET) surface area was measured by N_2 adsorption at 77 K using a volumetric gas adsorption apparatus (BELmini, Bel Japan, Inc.). The UV–vis diffuse reflectance (UV–vis DR) spectra were measured using a JASCO Corporation V-670 spectrometer equipped with an integrating sphere. Spectralon® filled with BaSO_4 , supplied by Labsphere Inc., was used as a reflection standard. SEM images were obtained from field emission scanning electron microscopy (FE-SEM, SU-8220, Hitachi High-Technologies) equipped with an energy-dispersive X-ray spectroscope (EDS) at an acceleration voltage of 3.0 kV. The XPS measurement was acquired using an X-ray photoelectron spectrometer (ESCA 3400, Shimadzu Corp.), and calibrated by the peak that can be assigned to C 1s.

2.3. Photocatalytic reduction of CO_2

The photocatalytic conversion of CO_2 by H_2O was carried out in a flow system using an inner-irradiation-type reaction vessel at room temperature and ambient pressure. The photocatalyst (1.0 g) was dispersed in ultrapure water (1.0 L) containing 0.1 mol of NaHCO_3 ,

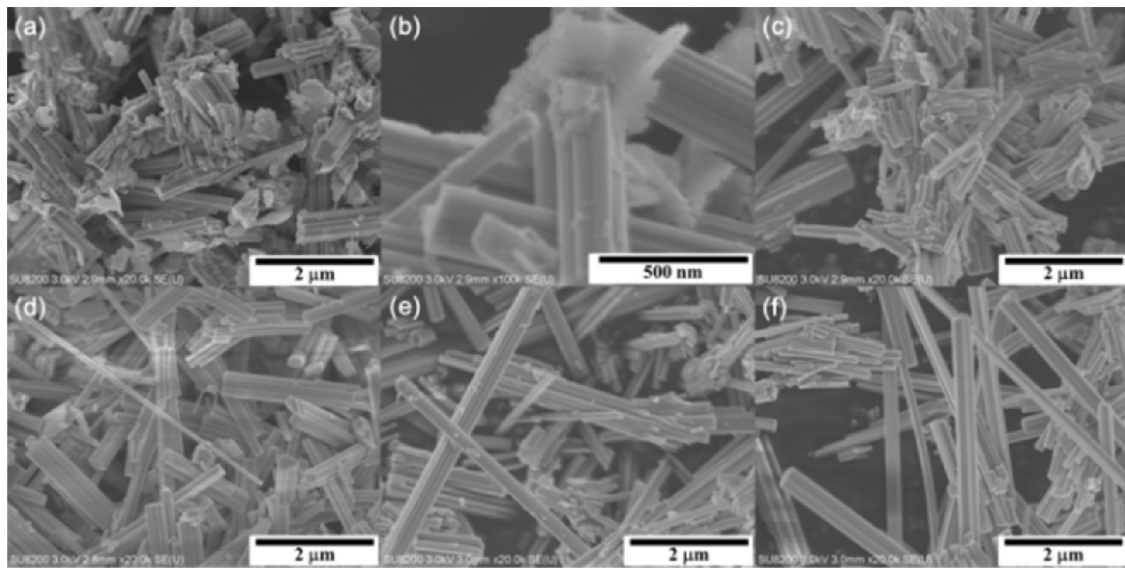


Fig. 2. SEM images of $\text{Sr}_2\text{KTa}_5\text{O}_{15}$ calcined at 1123 K (a and b), 1173 K (c), 1223 K (d), 1273 K (e), and 1373 K (f) for 3 h in KCl flux ($\text{F}/\text{P} = 2.0$).

and CO_2 gas (99.999%) was bubbled into the solution at a flow rate of 30 mL min^{-1} . The suspension was irradiated under a 400 W high-pressure mercury lamp with a quartz filter connected to a water cooling system. The generated gaseous products such as H_2 , O_2 , and CO were analyzed by thermal conductivity detector-gas chromatography (TCD-GC) using a GC-8A chromatograph (Shimadzu Corp.) equipped with a Molecular Sieve 5A column with Ar as the carrier gas and by flame ionization detector-gas chromatography (FID-GC) with a methanizer using a ShinCarbon ST column with N_2 as the carrier gas.

The selectivity toward CO evolution compared to H_2 evolution and the balance between consumed electrons (e^-) and holes (h^+) can generally be described using the formulae shown below:

$$\text{Selectivity toward CO evolution (\%)} = 100 \times R_{\text{CO}} / (R_{\text{CO}} + R_{\text{H}_2})$$

$$\text{Consumed } e^- / h^+ = (R_{\text{CO}} + R_{\text{H}_2}) / (2 \times R_{\text{O}_2})$$

where R_{CO} , R_{H_2} , and R_{O_2} represent the rate of formation of CO , H_2 , and O_2 , respectively.

3. Results and discussion

Taking into account that the melting point of KCl is approximately 1049 K, we calcined the mixture of KCl and precursors above 1100 K, in order to investigate the effect of calcination temperature on the physical and chemical properties of $\text{Sr}_2\text{KTa}_5\text{O}_{15}$. No obvious change was observed in the XRD patterns of $\text{Sr}_2\text{KTa}_5\text{O}_{15}$ with increasing temperature calcined from 1123 K to 1373 K, as shown in Fig. 1A. However, peaks assigned to a slight impurity phase are found in the 2θ range 24°–34° in the enlarged XRD pattern of $\text{Sr}_2\text{KTa}_5\text{O}_{15}$ calcined at 1123 K, as shown in Fig. 1B. The other peaks in the samples are consistent with those of TTB-type $\text{Sr}_2\text{KTa}_5\text{O}_{15}$ [24], which indicates that a pure phase of $\text{Sr}_2\text{KTa}_5\text{O}_{15}$ is obtained when KCl ($\text{F}/\text{P} = 2$) is used as flux at 1173 K for 3 h. The crystallite diameter was determined using the full width at half maximum (FWHM) of the (320) plane according to the Scherrer equation. The samples calcined at different temperatures showed similar crystallite diameters (Fig. 1C), which suggests that the calcination temperature does not promote crystallinity. On the other hand, the calcination temperature showed an obvious effect on the BET specific surface area, which decreased from 10.57 to 4.54 $\text{m}^2 \text{g}^{-1}$, as calcination temperature increased from 1123 K to 1373 K.

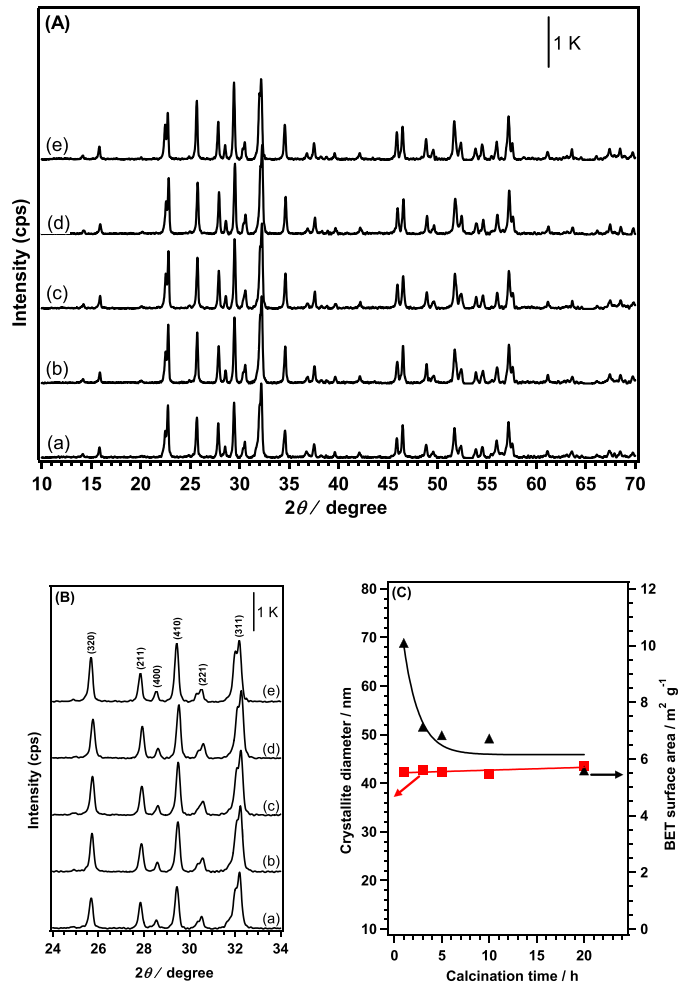


Fig. 3. (A) XRD patterns of $\text{Sr}_2\text{KTa}_5\text{O}_{15}$ calcined at 1173 K for 1 h (a), 3 h (b), 5 h (c), 10 h (d), and 20 h (e) in KCl flux ($\text{F}/\text{P} = 2.0$); (B) The enlarged XRD patterns of the above samples at the 2θ range from 24° to 34°; (C) Crystallite diameter of (320) plane and BET specific surface area of $\text{Sr}_2\text{KTa}_5\text{O}_{15}$ prepared at different calcination times.

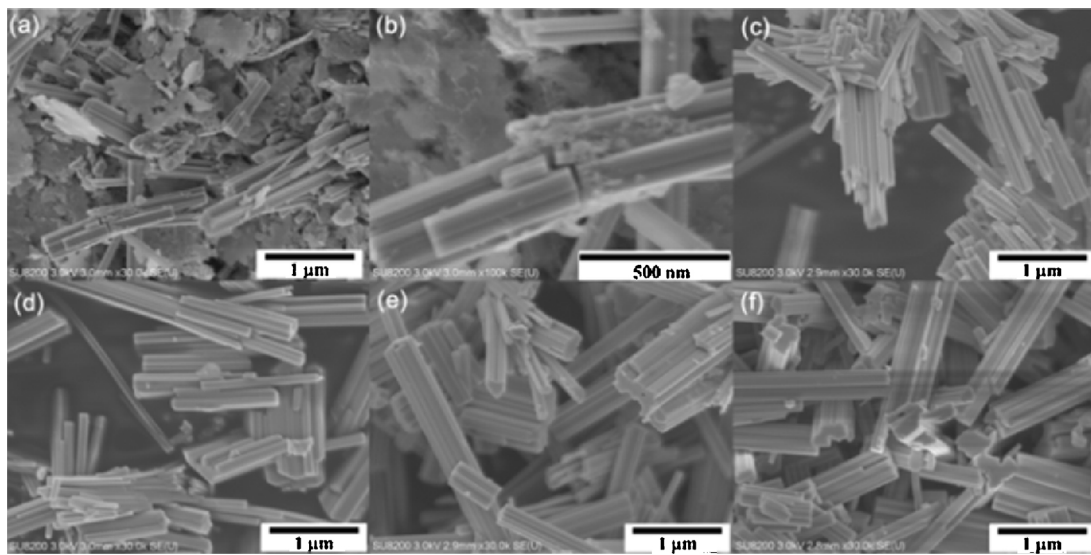


Fig. 4. SEM images of Sr₂KTa₅O₁₅ calcined at 1173 K for 1 h (a and b), 3 h (c), 5 h (d), 10 h (e), and 20 h (f) in KCl flux (F/P = 2.0).

SEM images of Sr₂KTa₅O₁₅ calcined at different temperatures for 3 h in KCl flux (F/P = 2) are shown in Fig. 2. For the sample calcined at 1123 K, two kinds of morphologies were found in the SEM images (Fig. 2(a) and (b)): nanorods and nanoplates. Only uniformed nanorods were observed when the calcination temperature increased to 1173 K (Fig. 2(c)). The diameters of the nanorods were in the range of 50–400 nm and the lengths were in the range of 1–3 μm. The length of the nanorods increased when the calcination temperature was increased from 1223 to 1273 K and reached to more than 4 μm, as shown in Fig. 2(d)–(f). From the SEM images, it is clear that the morphology of samples changes from a mixture of nanorods and nanoplates to nanorods only, and the lengths of these nanorods increase by several micrometers with increase in the calcination temperature.

The calcination time does not have an impact on the XRD pattern, but does have an impact on the morphology of Sr₂KTa₅O₁₅, as shown in Figs. 3 and 4. The pure phase of Sr₂KTa₅O₁₅ was obtained even when calcination was carried out at 1173 K for 1 h. No apparent change was observed in the XRD patterns with an increase in the calcination time from 1 to 20 h (Fig. 3A and B). The crystallite diameter showed a slight enhancement from 42.2 to 43.6 nm; however, the BET specific surface area showed a significant decrease with an increase in the calcining time from 1 to 5 h. Sr₂KTa₅O₁₅ calcined at 1173 K for 1 h showed the largest BET specific surface area (10.03 m² g⁻¹), while that of the other samples was only approximately 6 m² g⁻¹ (Fig. 3C).

The SEM image of the sample calcined at 1173 K for 1 h in KCl flux (F/P = 2) shows a structure with a large number of nanoplates and a small number of nanorods (Fig. 4(a) and (b)). Since there were no other phases except for the TTB phase according to the XRD patterns (Fig. 3A and B), these nanoplates should comprise either crystallized or amorphous Sr₂KTa₅O₁₅. EDS analysis of one nanoparticle indicated that K, Sr, Ta, and O elements were well mapped with its morphology (Fig. S1); therefore, we expect that these nanoplates are also Sr₂KTa₅O₁₅. Only nanorods were observed when the calcination time was increased to 3 h (Fig. 4(c)). The well-shaped Sr₂KTa₅O₁₅ nanorods were obtained when the samples were calcined at 1173 K for more than 3 h using KCl flux (F/P = 2) (Fig. 4(d)–(f)).

The mass ratio of flux (KCl to precursors) usually affects the morphology, phase, purity, and crystallinity of the products [25]. First, we compared the flux method with the SSR and PC methods for the fabrication of Sr₂KTa₅O₁₅. Interestingly, pure TTB structure of

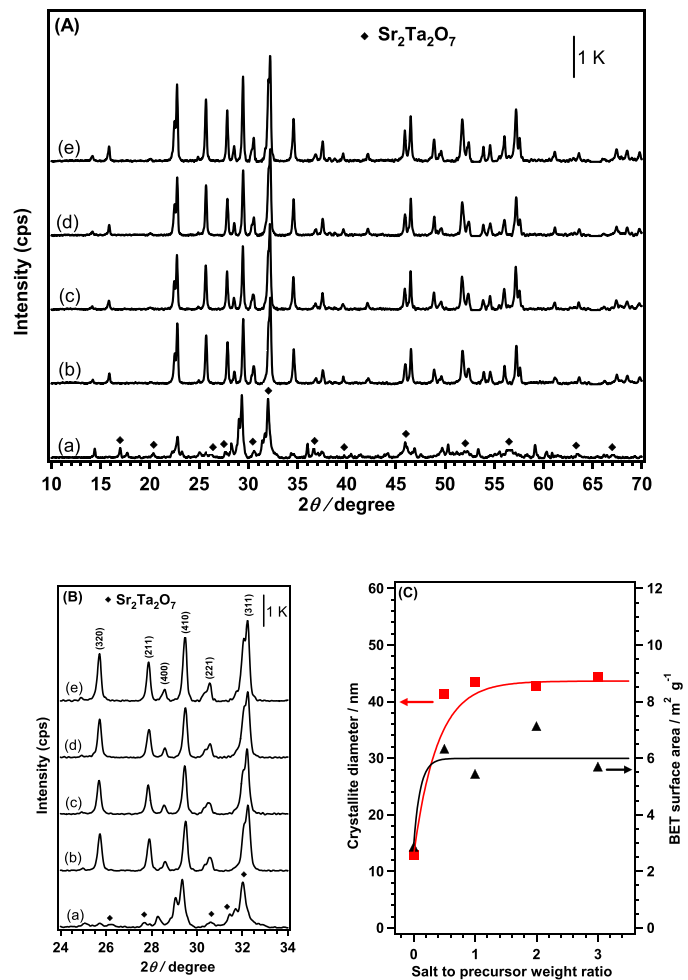


Fig. 5. (A) XRD patterns of Sr₂KTa₅O₁₅ calcined at 1173 K for 3 h in mass ratios of KCl flux to precursor (F/P) of 0 (a), 0.5 (b), 1.0 (c), 2.0 (d) and 3.0 (e); (B) The enlarged XRD patterns of the above amples at the 2θ range from 24° to 34°; (C) Crystallite diameter of (320) plane and BET specific surface area of Sr₂KTa₅O₁₅ prepared at different F/P ratios.

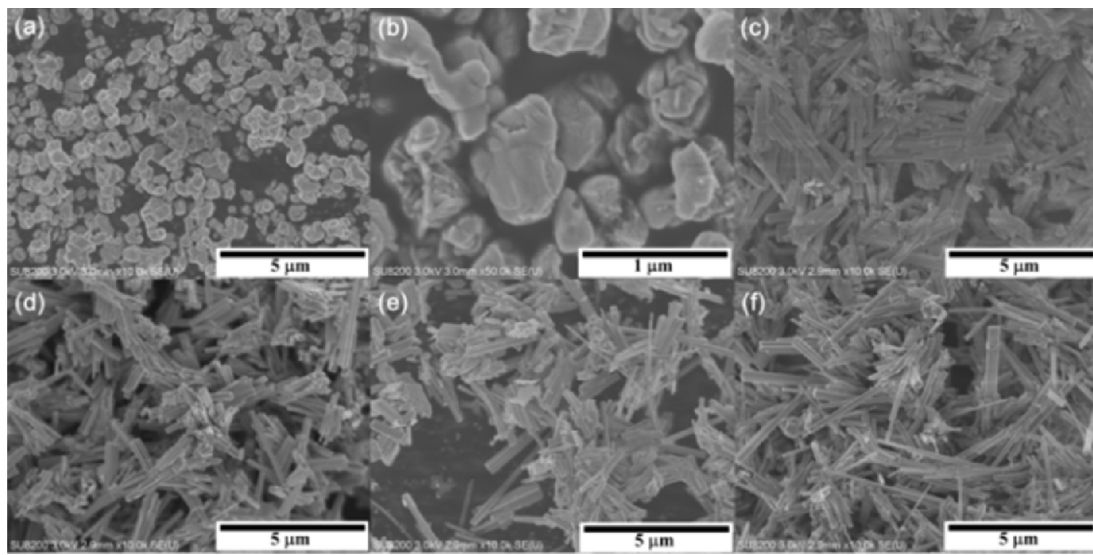


Fig. 6. SEM images of $\text{Sr}_2\text{KTa}_5\text{O}_{15}$ calcined at 1173 K for 3 h in mass ratio of KCl flux to precursors (F/P) of 0 (a and b), 0.5 (c), 1.0 (d), 2.0 (e) and 3.0 (f).

$\text{Sr}_2\text{KTa}_5\text{O}_{15}$ could not be obtained by the SSR and PC methods. The XRD patterns clearly show that a pure phase of $\text{Sr}_2\text{KTa}_5\text{O}_{15}$ is not obtained by the SSR method without any flux (Fig. 5A). The main phase is assigned to $\text{Sr}_2\text{Ta}_2\text{O}_7$ obtained after performing calcination for 3 h at 1173 K [26]. We tried to prepare $\text{Sr}_2\text{KTa}_5\text{O}_{15}$ at high temperatures and long calcination periods using the SSR method (e.g., 1173 K for 24 h); however, the pure phase of $\text{Sr}_2\text{KTa}_5\text{O}_{15}$ was still not obtained (Fig. S2(a)). PC method is one of the most famous methods for the fabrication of tantalates, and has been investigated by many researchers [23,27–29]. However, the pure phase of $\text{Sr}_2\text{KTa}_5\text{O}_{15}$ was still not obtained at 1173 K for 3 h using the PC method (Fig. S2(b)). These results indicate that both the SSR and PC methods are unsuitable for the fabrication of the pure phase of $\text{Sr}_2\text{KTa}_5\text{O}_{15}$ at 1173 K for 3 h. However, the pure phase of $\text{Sr}_2\text{KTa}_5\text{O}_{15}$ was obtained even with the low ratio of KCl flux (F/P = 0.5) at 1173 K for 3 h. Further increasing the F/P ratio from 1.0 to 3.0 did not cause any obvious phase change (Fig. 5B). $\text{Sr}_2\text{KTa}_5\text{O}_{15}$ fabricated by the SSR method (without KCl flux) showed the lowest crystallite diameter and BET specific surface area amongst all the samples (Fig. 5C). This can be explained by the fact that the particles are sintered easily by using the SSR method. In contrast, $\text{Sr}_2\text{KTa}_5\text{O}_{15}$ fabricated by the flux method in different F/P ratios showed similar crystallite diameters and BET specific surface areas, indicating that these physical properties are influenced by the presence or absence of flux but not by the F/P ratio.

Fig. 6 shows the SEM images of $\text{Sr}_2\text{KTa}_5\text{O}_{15}$ prepared by calcination at 1173 K for 3 h in different F/P ratios. The morphology of $\text{Sr}_2\text{KTa}_5\text{O}_{15}$ fabricated by the SSR method (F/P = 0) at 1173 K for 3 h displayed irregular nanoparticles of 0.5–1 μm diameters (Fig. 6(a) and (b)). nanoparticles of large sizes were obtained by the SSR method at 1173 K for 24 h without flux (Fig. S3(a)), whereas nanoparticles of similar morphology were obtained by the PC method at 1173 K for 3 h (Fig. S3(b)). However, only nanorods were observed in the samples fabricated by the flux method (Fig. 6(c)–(f)). Despite increasing the F/P ratio from 0.5 to 2.0, the length of these nanorods did not change significantly, further increasing the F/P ratio to 3.0 increased the length of nanorods (Fig. 6(f)). Based on the analysis above, it can be concluded that KCl flux plays an essential role in the growth of $\text{Sr}_2\text{KTa}_5\text{O}_{15}$ nanorods.

In order to obtain information about elemental distribution for the $\text{Sr}_2\text{KTa}_5\text{O}_{15}$ nanorods, EDS analysis was carefully performed. Fig. 7 shows the results of the EDS analysis of a $\text{Sr}_2\text{KTa}_5\text{O}_{15}$ nanorod fabricated at 1173 K for 3 h in KCl flux (F/P = 2). The evenly dis-

tributed points of the related K, Sr, Ta, and O elements indicate that the $\text{Sr}_2\text{KTa}_5\text{O}_{15}$ crystal has a homogeneous composition. All the elements can also be clearly seen in the corresponding spectrum shown in Fig. 7(f). Based on the XRD, SEM, and EDS results, there is no doubt that the well-shaped $\text{Sr}_2\text{KTa}_5\text{O}_{15}$ nanorod is easily prepared using KCl flux for a short duration.

Fig. 8 shows the UV-vis DR spectra of $\text{Sr}_2\text{KTa}_5\text{O}_{15}$ prepared under various conditions. The samples calcined at different temperatures and times (Fig. 8(a) and (b)) show almost the same absorption edge at approximately 310 nm, which indicates that the calcination temperature and times have almost no effect on the band gap. Fig. 8C shows the UV-vis DR spectra of $\text{Sr}_2\text{KTa}_5\text{O}_{15}$ calcined at 1173 K for 3 h at different F/P ratios. The absorption edge in the UV-vis DR spectra of $\text{Sr}_2\text{KTa}_5\text{O}_{15}$ fabricated by the SSR method (300 nm) is lower than that of the flux method (310 nm). Moreover, all the materials fabricated by using the flux method showed a similar absorption edge at around 310 nm, indicating that materials prepared using different flux ratios showed no obvious effect on the band gap. Fig. 8D shows 1.0 wt% Ag-loaded $\text{Sr}_2\text{KTa}_5\text{O}_{15}$ sample fabricated at 1173 K for 3 h in KCl flux (F/P = 2). The broad absorption band from 330 to 650 nm is owing to the surface plasmon absorption of Ag nanoparticles deposited by a chemical reduction method [16–19,22,23].

The fabricated $\text{Sr}_2\text{KTa}_5\text{O}_{15}$ nanorods with 1.0 wt% Ag cocatalyst exhibited activity for the photocatalytic conversion of CO_2 by H_2O under UV irradiation (Fig. 9A). An almost stoichiometric formation rate of O_2 as an oxidation product together with those of CO and H_2 as reduction products were obtained in all cases, which indicates that H_2O works as an electron donor for the photocatalytic conversion of CO_2 . All the components of the system, i.e., photocatalyst, photoirradiation, CO_2 bubbling, a Ag cocatalyst, and a NaHCO_3 additive, are necessary to achieve the highly selective conversion of CO_2 into CO . We carried out five blank tests by keeping one component absent in each test and performed the reaction. We observed that $\text{Sr}_2\text{KTa}_5\text{O}_{15}$ with the Ag cocatalyst in an aqueous solution of NaHCO_3 with bubbling CO_2 under photoirradiation can consistently achieve a high formation rate of CO and good selectivity toward CO evolution in the photocatalytic conversion of CO_2 by H_2O , as shown in Fig. 9A. Without the NaHCO_3 additive, water splitting proceeded as the dominant reaction, leading to the evolution of the highest formation rate of H_2 (Fig. 9B). Carbonate species might play an important role in desorption of O_2 during photocatalytic water splitting, which was reported by Sayama et al. [30]. In our

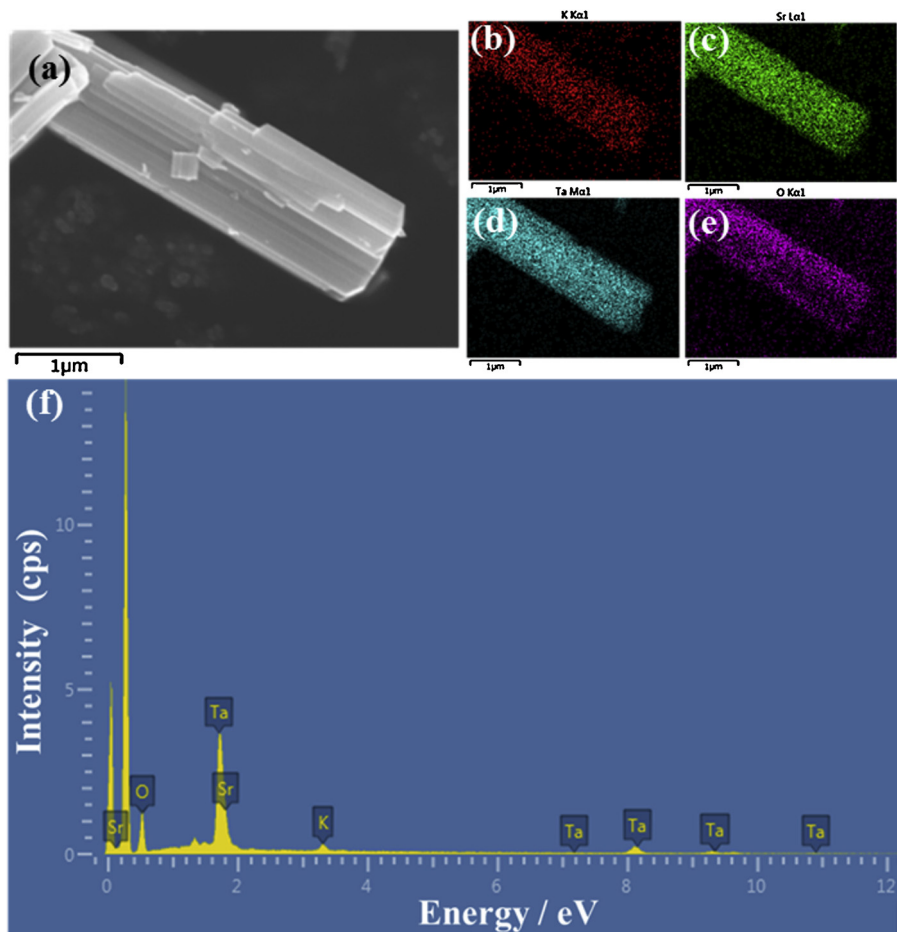


Fig. 7. EDS analysis of $\text{Sr}_2\text{KTa}_5\text{O}_{15}$ prepared at 1173 K for 3 h in KCl flux ($\text{F}/\text{P} = 2.0$): (a) selected SEM image, (b) K mapping image, (c) Sr mapping image, (d) Ta mapping image, (e) O mapping image and (f) corresponding spectrum.

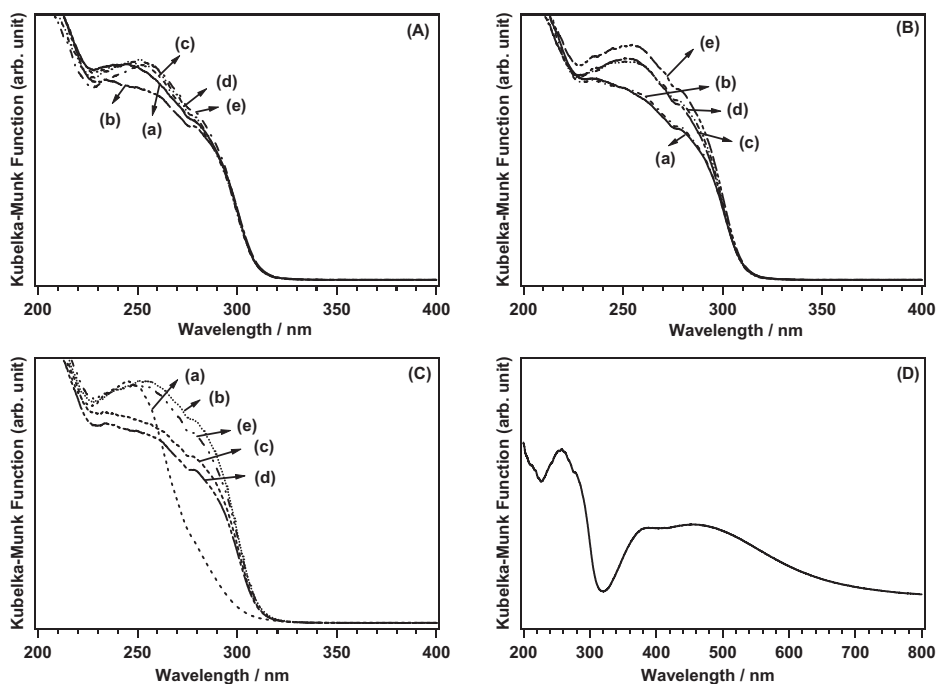


Fig. 8. UV-vis DR spectra of $\text{Sr}_2\text{KTa}_5\text{O}_{15}$ (A) calcined for 3 h in KCl flux at 1123 K (a), 1173 K (b), 1223 K (c), 1273 K (d), and 1373 K (e) for 3 h in KCl flux ($\text{F}/\text{P} = 2.0$); (B) calcined at 1173 K for 1 h (a), 3 h (b), 5 h (c), 10 h (d), and 20 h (e) in KCl flux ($\text{F}/\text{P} = 2$); (C) calcined at 1173 K for 3 h in mass ratio of KCl flux to precursor (F/P) of 0 (a), 0.5 (b), 1.0 (c), 2.0 (d), 3.0 (e) and (D) calcined at 1173 K for 3 h in mass ratio of KCl flux to precursor (F/P) of 2.0 with 1.0 wt% Ag-loaded.

system, NaHCO_3 might also play such kind of function, which leads to the suppression of the H_2 generation when flowing CO_2 . Similarly, without the Ag cocatalyst, H_2 was the main product, while the evolution of CO was very low (Fig. 9C). This indicates that the Ag cocatalyst is an important factor in the photocatalytic conversion of CO_2 in an aqueous solution of NaHCO_3 . When inert Ar gas was used instead of CO_2 , maximum photocatalytic water splitting was observed and only a very small amount of CO derived from NaHCO_3 was formed (Fig. 9D). This indicates that CO_2 acts not only as a carbon source, but also as a balance gas to maintain the concentration of the HCO_3^- ion, which provides suitable pH values for the photocatalytic conversion of CO_2 by H_2O . In the absence of a photocatalyst or photoirradiation (Fig. 9E and F), almost no products were detected.

Fig. 10A shows the formation rates of CO, O_2 , and H_2 for the photocatalytic conversion of CO_2 by H_2O over $\text{Sr}_2\text{KTa}_5\text{O}_{15}$ nanoplates and nanorods calcined at different temperatures for 3 h in KCl flux ($\text{F}/\text{P}=2$) and characterized by XRD, BET analysis, and SEM, as shown in Figs. 1 and 2. $\text{Sr}_2\text{KTa}_5\text{O}_{15}$ calcined at 1123 K for 3 h in KCl flux ($\text{F}/\text{P}=2$) exhibited the lowest formation rate of CO ($38.2 \mu\text{mol h}^{-1}$) and the highest formation rate of H_2 ($43.2 \mu\text{mol h}^{-1}$), resulting in a selectivity of only 46.9% toward CO evolution. When the calcination temperature was increased by only 50 K to up to 1173 K, the formation rate of CO increased to $63.0 \mu\text{mol h}^{-1}$, while the formation rate of H_2 was significantly suppressed to only $12.6 \mu\text{mol h}^{-1}$. The resulting selectivity toward CO evolution dramatically increased to 83.3%. This result implies that the mixture of $\text{Sr}_2\text{KTa}_5\text{O}_{15}$ nanoplates and nanorods containing an unknown impurity, even with the highest BET specific surface area, exhibits activity in favor of water splitting and not for the photocatalytic conversion of CO_2 by H_2O . Increasing the calcination temperature from 1223 K to 1373 K led to a slight decrease in the photocatalytic activity for the formation rate of CO, which might be due to the decrease in the BET specific surface area and the increase in the length of the nanorods [31]. Overall, these results indicate that the $\text{Sr}_2\text{KTa}_5\text{O}_{15}$ nanorods prepared using a flux method show high formation rates of CO and good selectivity toward CO evolution.

Fig. 10B shows the formation rates of CO, O_2 , and H_2 for the photocatalytic conversion of CO_2 by H_2O over $\text{Sr}_2\text{KTa}_5\text{O}_{15}$ nanoplates and nanorods calcined for different calcination periods at 1173 K in KCl flux ($\text{F}/\text{P}=2$), and were characterized by XRD, BET analysis, and SEM, as shown in Figs. 3 and 4. The $\text{Sr}_2\text{KTa}_5\text{O}_{15}$ calcined for 1 h comprised a mixture of nanoplates and nanorods and showed the lowest formation rate of CO ($42.8 \mu\text{mol h}^{-1}$). This result was similar to that observed when the $\text{Sr}_2\text{KTa}_5\text{O}_{15}$ particles were calcined at 1123 K for 3 h. We can therefore conclude that the important factor for obtaining a high formation rate of CO and good selectivity toward CO evolution is the formation of pure nanorods, and not a high BET specific surface area. Increasing the calcination duration from 5 to 20 h led to a slight decrease in the formation rate of CO and an increase of the formation rate of H_2 .

Fig. 10C shows the formation rates of CO, O_2 , and H_2 for the photocatalytic conversion of CO_2 by H_2O over $\text{Sr}_2\text{KTa}_5\text{O}_{15}$ nanoparticles and nanorods calcined in different F/P ratios at 1173 K for 3 h and characterized by XRD, BET analysis, and SEM, as shown in Figs. 5 and 6. A F/P ratio of 0 means that the sample was fabricated using the SSR method (without flux). The F/P=0 sample comprising mainly of $\text{Sr}_2\text{Ta}_2\text{O}_7$ nanoparticles showed the lowest selectivity toward CO evolution (48.4%) among all the samples with different mass ratios of flux. The low formation rate of CO ($44 \mu\text{mol h}^{-1}$) indicates that we did not observe a high formation rate of CO or a good selectivity toward CO evolution in the absence of pure phase $\text{Sr}_2\text{KTa}_5\text{O}_{15}$. We also carried out the photocatalytic conversion of CO_2 by H_2O over $\text{Sr}_2\text{KTa}_5\text{O}_{15}$ fabricated by the SSR method at 1773 K for 24 h. However, such a high calcination temperature

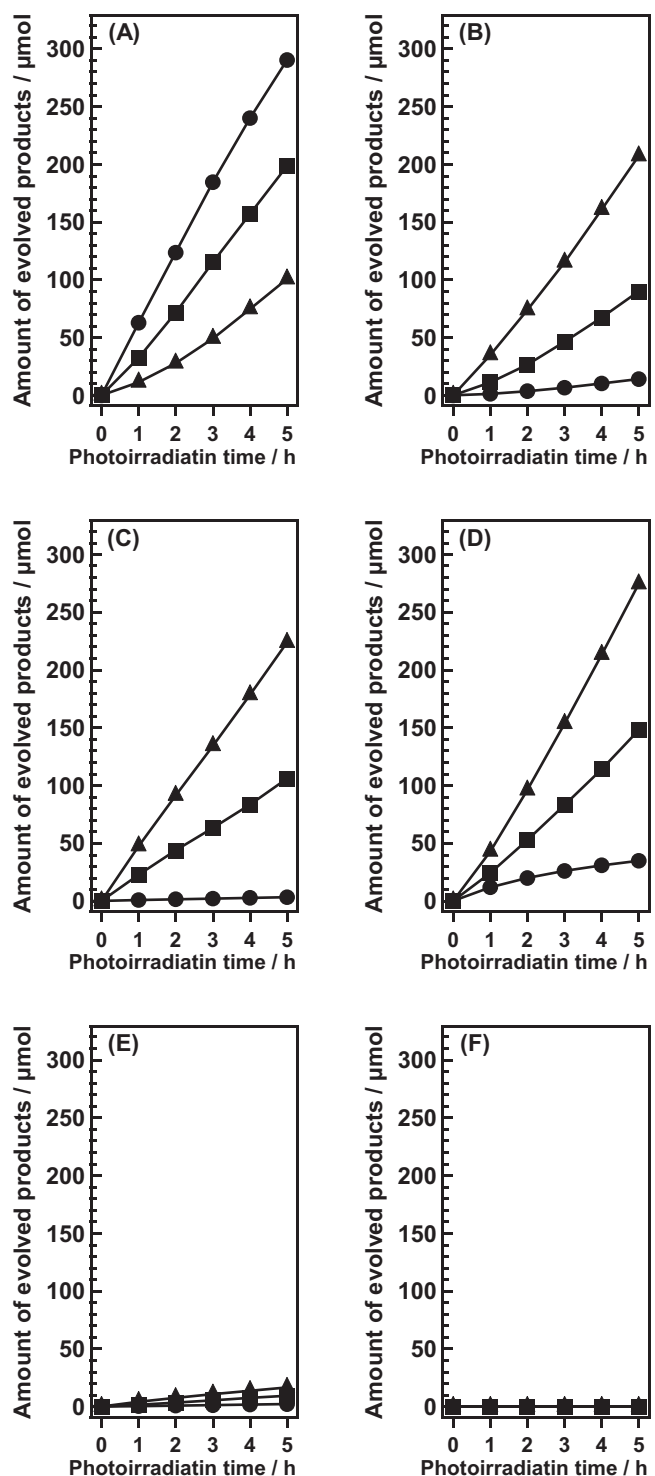


Fig. 9. Time course of CO (circle), O_2 (square), and H_2 (triangle) evolutions over $\text{Sr}_2\text{KTa}_5\text{O}_{15}$ calcined at 1173 K for 3 h in KCl flux ($\text{F}/\text{P}=2$) under 5 h under typical condition (A), without a NaHCO_3 additive (B), without a Ag cocatalyst (C), with Ar flow at rate of 30 mL min^{-1} (D), without a catalyst (E), and without photoirradiation (F).

and long calcination duration led to a very small BET specific surface area ($0.5 \text{ m}^2 \text{ g}^{-1}$) and very low photocatalytic activity (Table S1(a)). Pure phase of $\text{Sr}_2\text{Ta}_2\text{O}_7$ was obtained by using SrCl_2 as flux at 1273 K for 6 h (Fig. S2(c)), which was similar to the findings reported elsewhere [26]. The as-fabricated $\text{Sr}_2\text{Ta}_2\text{O}_7$ mainly showed activity for the overall water splitting reaction under the

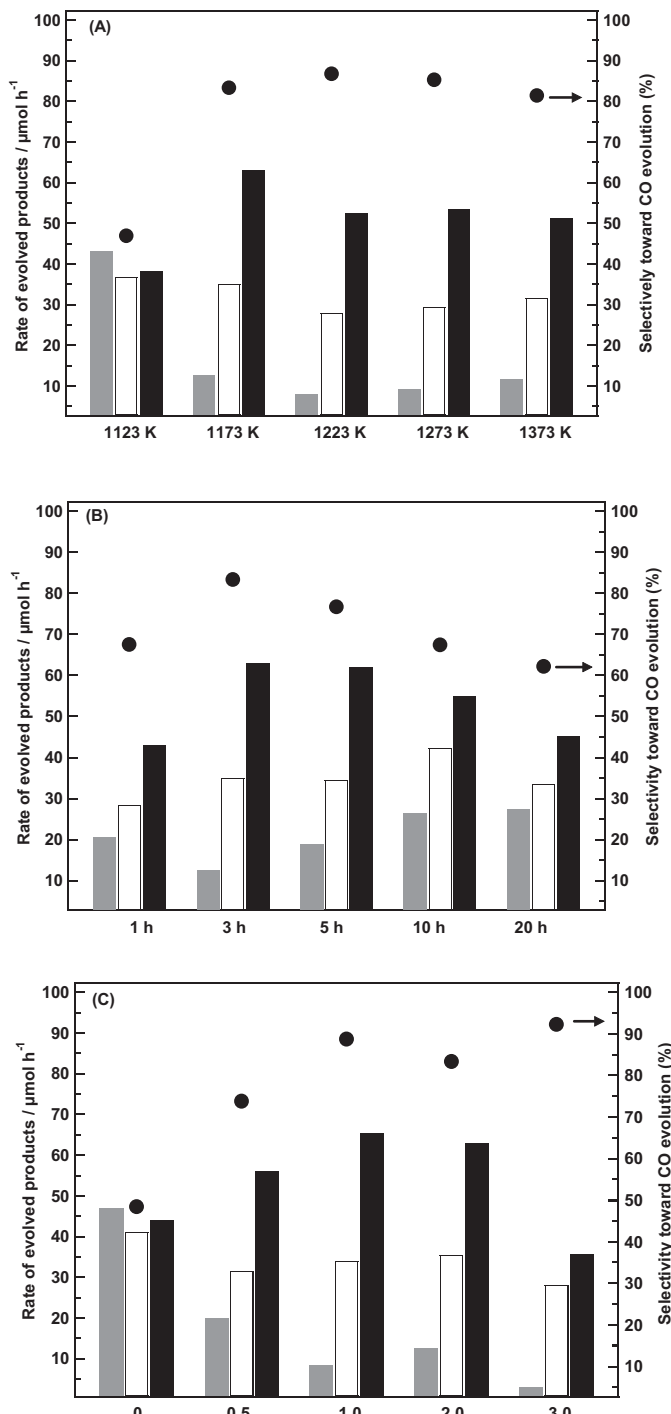


Fig. 10. Formation rates of CO (black), O₂ (white), and H₂ (gray) and selectivity toward CO evolution over $\text{Sr}_2\text{KTa}_5\text{O}_{15}$ calcined at different calcination temperatures for 3 h in KCl flux (F/P = 2) (A); calcined for different calcination periods at 1173 K in KCl flux (F/P = 2) (B); calcined in different F/P ratios at 1173 K for 3 h in KCl flux (C). Amount of catalyst: 1.0 g, loading amount of cocatalyst: 1.0 wt% Ag cocatalyst loaded by the chemical reduction method, light source: 400 W high-pressure mercury lamp, volume of water: 1.0 L, CO_2 flow rate: 30 mL min^{-1} , additive: NaHCO_3 (0.1 mol L^{-1}).

same reaction conditions, along with a very low formation rate of CO (Table S1(b)). $\text{Sr}_2\text{KTa}_5\text{O}_{15}$ fabricated by the SSR method, which contained $\text{Sr}_2\text{Ta}_2\text{O}_7$ as an impurity, showed mostly photocatalytic activity for H₂ evolution (Fig. 10C at F/P = 0 and Table S1(a)). Based on these two results, we concluded that $\text{Sr}_2\text{Ta}_2\text{O}_7$ works as a photocatalyst for the overall water splitting reaction. Sample with the

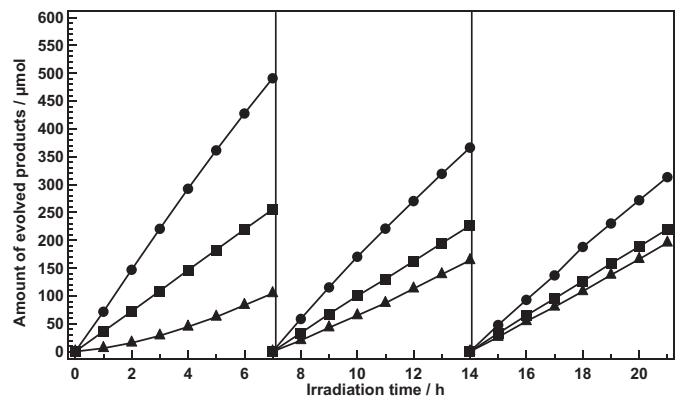


Fig. 11. Time courses of CO (circle), O₂ (square), and H₂ (triangle) evolutions for the photocatalytic conversion of CO_2 by H_2O over the Ag-modified $\text{Sr}_2\text{KTa}_5\text{O}_{15}$ nanorods calcined at 1173 K for 3 h in KCl (F/P = 1) flux. Amount of catalyst: 1.0 g, loading amount of cocatalyst: 1.0 wt% Ag cocatalyst loaded by the chemical reduction method, light source: 400 W high-pressure mercury lamp, volume of water: 1.0 L, CO_2 flow rate: 30 mL min^{-1} , additive: NaHCO_3 (0.1 mol L^{-1}).

phase of $\text{Sr}_2\text{Ta}_2\text{O}_7$ impurity then leads to low photocatalytic activity for CO_2 conversion to CO using H_2O as an electron donor.

The formation rate of CO increased and that of H₂ dramatically suppressed over $\text{Sr}_2\text{KTa}_5\text{O}_{15}$ fabricated by the flux method, as compared to that prepared by the SSR method. Flux method as a simple and cost-effective way to fabricate well-shaped and well-crystallized particles has been widely investigated [25,32,33]. $\text{Sr}_2\text{KTa}_5\text{O}_{15}$ nanorods fabricated in KCl flux in a lower calcination temperature and shorter time showed the highest photocatalytic activity and good selectivity toward CO evolution comparing with that of samples fabricated using SSR method. This might be due to the formation of regular morphology of photocatalyst, these nanorods were grown along the [001] direction, which was reported by Wang et al. [24]. The nanorods were also reported to be more efficiency for migration of photogenerated electrons and holes than that of nanoparticles [23], which should be responsible for the high photocatalytic activity of CO_2 conversion by H_2O . The formation rate of CO and selectivity toward CO evolution increased with an increase in the F/P ratio and reached a maximum at F/P = 1.0. Further increase in the F/P ratio to 3.0 led to a significant decrease in the photocatalytic activity toward CO evolution. The $\text{Sr}_2\text{KTa}_5\text{O}_{15}$ nanorods fabricated at F/P = 1.0 showed the highest photocatalytic activity toward CO evolution at 65.5 $\mu\text{mol h}^{-1}$ and good selectivity toward CO evolution (88.7%) among all the samples.

Fig. 11 shows the time course of H₂, O₂, and CO evolutions for the photocatalytic conversion of CO_2 by H_2O over the Ag-modified $\text{Sr}_2\text{KTa}_5\text{O}_{15}$ nanorods calcined at 1173 K for 3 h in KCl flux (F/P = 1), which represents the optimal fabrication conditions. CO was evolved as the main reduction product, and a small amount of H₂ was generated during the first run. Simultaneously, the evolution of O₂ increased linearly during the reaction. The evolution of CO, H₂, and O₂ are in an approximately stoichiometric ratio, indicating that the number of photo-electrons used for the reduction of CO_2 and protons is equivalent to the number of holes consumed for H_2O oxidation. It was observed that the formation rate of CO decreased together with a small increase in the formation rate of H₂, during the second and third runs. However, it should be noted that the main product of the photocatalytic reduction was still CO even during the third run, indicating that CO was produced in preference to H₂.

Fig. 12a and b show the SEM images of the Ag-modified $\text{Sr}_2\text{KTa}_5\text{O}_{15}$ nanorod calcined at 1173 K for 3 h in KCl (F/P = 1) flux before and after the photocatalytic conversion of CO_2 by H_2O . It was clearly seen that Ag nanoparticles were well anchored on

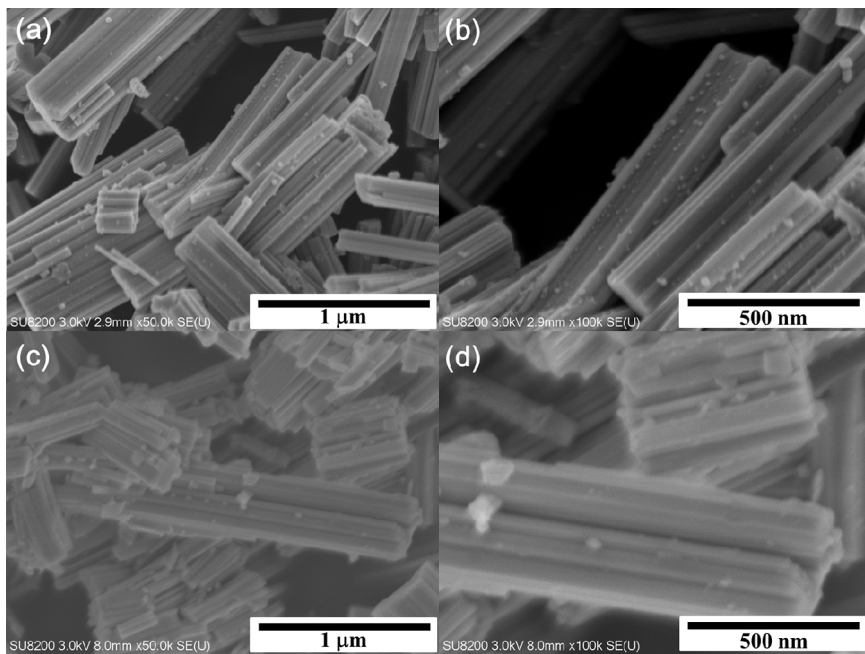


Fig. 12. SEM images of the Ag-modified $\text{Sr}_2\text{KTa}_5\text{O}_{15}$ nanorods calcined at 1173 K for 3 h in KCl ($\text{F}/\text{P} = 1$) flux before (a and b) and after (c and d) the photocatalytic conversion of CO_2 by H_2O .

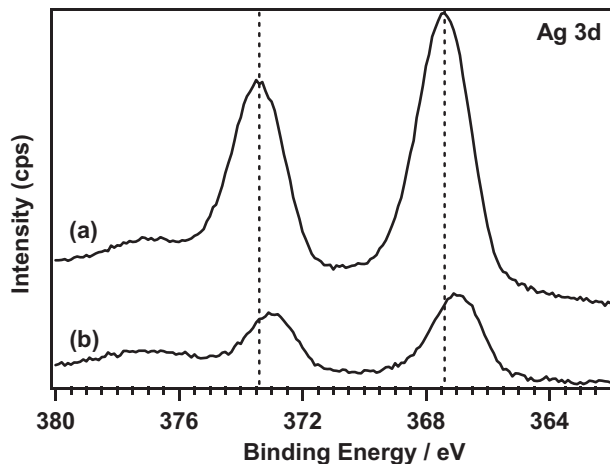


Fig. 13. X-ray photoelectron spectra of Ag-modified $\text{Sr}_2\text{KTa}_5\text{O}_{15}$ nanorods calcined at 1173 K for 3 h in KCl ($\text{F}/\text{P} = 1$) flux before (a) and after (b) the photocatalytic conversion of CO_2 by H_2O .

the nanorods, and the size of these Ag nanoparticles is 5–30 nm (Fig. S4a). We have previously reported that only the smaller Ag nanoparticles contribute to the high selectivity toward CO evolution and the subsequent evolution of stoichiometric amounts of O_2 for the photocatalytic conversion of CO_2 by H_2O over $\text{Ag}/\text{SrO}/\text{Ta}_2\text{O}_5$ [19]. However, the size of Ag nanoparticles after photoirradiation was increased to 20–80 nm (Fig. S4b), which was much larger than that before the photoirradiation, on the other hand, the number of Ag anchored on the surface of nanorods were decreased (Fig. 12c and d), which should be due to re-photodeposition and aggregation of the Ag nanoparticles. Ag nanoparticles are known to easily leach into a solution as Ag^+ ions under photoirradiation [34].

Fig. 13 shows Ag 3d X-ray photoelectron spectra (XPS) of Ag-modified $\text{Sr}_2\text{KTa}_5\text{O}_{15}$ nanorods calcined at 1173 K for 3 h in KCl ($\text{F}/\text{P} = 1$) flux before the photocatalytic conversion of CO_2 by H_2O . Ag 3d5/2 and 3d3/2 peaks appeared at binding energies of 367.4 and 373.4 eV, respectively. The 3d peaks of Ag are doublets with energy

separation of 6.0 eV. This indicates that the metallic Ag nanoparticles are dispersed on the surface of $\text{Sr}_2\text{KTa}_5\text{O}_{15}$ [35]. The Ag 3d XPS after the reaction showed an obvious decrease of peak intensity. The percentage of Ag/Ta atom after the reaction was 6%, which was much smaller than that before the reaction (Ag/Ta = 17%), implying the dissolution of Ag during the photocatalytic reaction. It is also noted that the Ag 3d5/2 and 3d3/2 peaks shift to a lower binding energy after the reaction, which indicates that zerovalent Ag changed into monovalent Ag [36]. From the results of SEM and XPS, the sudden decline in the formation rate of CO evolution is attributed to the aggregation and dissolution of Ag nanoparticles as cocatalysts. Based on these analyses, we conclude that it is important to ensure that the cocatalyst consist of highly dispersed Ag nanoparticles anchored on the surface of the $\text{Sr}_2\text{KTa}_5\text{O}_{15}$ nanorods, and that the pH value is controlled in an aqueous solution of NaHCO_3 , in order to ensure a stable rate of formation of CO.

4. Conclusions

The $\text{Sr}_2\text{KTa}_5\text{O}_{15}$ nanorods, synthesized by a facile flux method using potassium chloride (KCl) as flux with a Ag cocatalyst, showed a high rate of formation of CO and good selectivity toward CO evolution, in the photocatalytic conversion of CO_2 by H_2O . The photocatalytic activity was significantly affected by the preparation methods, calcination temperature, calcination time, and ratio of flux to the precursors. As compared to the SSR and PC methods, the flux method not only generates pure phase $\text{Sr}_2\text{KTa}_5\text{O}_{15}$ at low calcination temperatures and short calcination durations, but also achieves a high formation rate of CO and good selectivity toward CO evolution.

Acknowledgements

This study was partially supported by a Grant-in-Aid for Scientific Research on Innovative Areas "All Nippon Artificial Photosynthesis Project for Living Earth" (No. 2406) of the Ministry of Education, Culture, Sports, Science, and Technology (MEXT) of Japan, the Precursory Research for Embryonic Science and Tech-

nology (PRESTO), supported by the Japan Science and Technology Agency (JST), and the Program for Elements Strategy Initiative for Catalysts & Batteries (ESICB), commissioned by the MEXT of Japan. Zeai Huang thanks the State Scholarship of China Scholarship Council, affiliated with the Ministry of Education of the P.R. China.

Appendix A. Supplementary data

Supplementary data associated with this article can be found, in the online version, at <http://dx.doi.org/10.1016/j.apcatb.2016.06.039>.

References

- [1] D.J. Hofmann, J.H. Butler, P.P. Tans, A new look at atmospheric carbon dioxide, *Atmos. Environ.* 43 (2009) 2084–2086.
- [2] M. Aresta, A. Dibenedetto, A. Angelini, Catalysis for the valorization of exhaust carbon: from CO_2 to chemicals, materials, and fuels. Technological use of CO_2 , *Chem. Rev.* 114 (2013) 1709–1742.
- [3] B. Kumar, M. Llorente, J. Froehlich, T. Dang, A. Sathrum, C.P. Kubiak, Photochemical and photoelectrochemical reduction of CO_2 , *Annu. Rev. Phys. Chem.* 63 (2012) 541–569.
- [4] R.K. Yadav, G.H. Oh, N.-J. Park, A. Kumar, K.-J. Kong, J.-O. Baeg, Highly selective solar-driven methanol from CO_2 by a photocatalyst/biocatalyst integrated system, *J. Am. Chem. Soc.* 136 (2014) 16728–16731.
- [5] T. Sakakura, J.-C. Choi, H. Yasuda, Transformation of carbon dioxide, *Chem. Rev.* 107 (2007) 2365–2387.
- [6] O.K. Varghese, M. Paulose, T.J. LaTempa, C.A. Grimes, High-rate solar photocatalytic conversion of CO_2 and water vapor to hydrocarbon fuels, *Nano Lett.* 9 (2009) 731–737.
- [7] J. Hemminger, R. Carr, G. Somorjai, The photoassisted reaction of gaseous water and carbon dioxide adsorbed on the SrTiO_3 (111) crystal face to form methane, *Chem. Phys. Lett.* 57 (1978) 100–104.
- [8] T. Inoue, A. Fujishima, S. Konishi, K. Honda, Photoelectrocatalytic reduction of carbon dioxide in aqueous suspensions of semiconductor powders, *Nature* 277 (1979) 637–638.
- [9] L. Liu, H. Zhao, J.M. Andino, Y. Li, Photocatalytic CO_2 reduction with H_2O on TiO_2 nanocrystals: comparison of anatase, rutile, and brookite polymorphs and exploration of surface chemistry, *ACS Catal.* 2 (2012) 1817–1828.
- [10] S.C. Roy, O.K. Varghese, M. Paulose, C.A. Grimes, Toward solar fuels: photocatalytic conversion of carbon dioxide to hydrocarbons, *ACS Nano* 4 (2010) 1259–1278.
- [11] S. Navalón, A. Dhakshinamoorthy, M. Álvaro, H. Garcia, Photocatalytic CO_2 reduction using non-titanium metal oxides and sulfides, *ChemSusChem* 6 (2013) 562–577.
- [12] S. Xie, Y. Wang, Q. Zhang, W. Deng, Y. Wang, MgO- and Pt-promoted TiO_2 as an efficient photocatalyst for the preferential reduction of carbon dioxide in the presence of water, *ACS Catal.* 4 (2014) 3644–3653.
- [13] L. Matějová, K. Kočí, M. Reli, L. Čapek, A. Hospodková, P. Peikertová, Z. Matěj, L. Obalová, A. Wach, P. Kuśtrowski, Preparation, characterization and photocatalytic properties of cerium doped TiO_2 : on the effect of Ce loading on the photocatalytic reduction of carbon dioxide, *Appl. Catal. B: Environ.* 152 (2014) 172–183.
- [14] W.-N. Wang, W.-J. An, B. Ramalingam, S. Mukherjee, D.M. Niedzwiedzki, S. Gangopadhyay, P. Biswas, Size and structure matter: enhanced CO_2 photoreduction efficiency by size-resolved ultrafine Pt nanoparticles on TiO_2 single crystals, *J. Am. Chem. Soc.* 134 (2012) 11276–11281.
- [15] W. Tu, Y. Zhou, Z. Zou, Photocatalytic conversion of CO_2 into renewable hydrocarbon fuels: state-of-the-art accomplishment, challenges, and prospects, *Adv. Mater.* 26 (2014) 4607–4626.
- [16] K. Teramura, Z. Wang, S. Hosokawa, Y. Sakata, T. Tanaka, A doping technique that suppresses undesirable H_2 evolution derived from overall water splitting in the highly selective photocatalytic conversion of CO_2 in and by water, *Chem.-A Eur. J.* 20 (2014) 9906–9909.
- [17] Z. Wang, K. Teramura, S. Hosokawa, T. Tanaka, Highly efficient photocatalytic conversion of CO_2 into solid CO using H_2O as a reductant over Ag-modified ZnGa_2O_4 , *J. Mater. Chem. A* 3 (2015) 11313–11319.
- [18] Z. Wang, K. Teramura, S. Hosokawa, T. Tanaka, Photocatalytic conversion of CO_2 in water over Ag-modified $\text{La}_2\text{Ti}_2\text{O}_7$, *Appl. Catal. B: Environ.* 163 (2015) 241–247.
- [19] K. Teramura, H. Tatsumi, Z. Wang, S. Hosokawa, T. Tanaka, Photocatalytic conversion of CO_2 by H_2O over Ag-loaded SrO -modified Ta_2O_5 , *Bull. Chem. Soc. Jpn.* 88 (2015) 431–437.
- [20] Y. Hori, H. Wakebe, T. Tsukamoto, O. Koga, Electrocatalytic process of CO selectivity in electrochemical reduction of CO_2 at metal electrodes in aqueous media, *Electrochim. Acta* 39 (1994) 1833–1839.
- [21] K. Iizuka, T. Wato, Y. Miseki, K. Saito, A. Kudo, Photocatalytic reduction of carbon dioxide over Ag cocatalyst-loaded $\text{AlA}_4\text{Ti}_4\text{O}_{15}$ (A = Ca, Sr, and Ba) using water as a reducing reagent, *J. Am. Chem. Soc.* 133 (2011) 20863–20868.
- [22] T. Takayama, K. Tanabe, K. Saito, A. Iwase, A. Kudo, The $\text{KCaSrTa}_5\text{O}_{15}$ photocatalyst with tungsten bronze structure for water splitting and CO_2 reduction, *Phys. Chem. Chem. Phys.* 16 (2014) 24417–24422.
- [23] T. Takayama, A. Iwase, A. Kudo, Photocatalytic water splitting and CO_2 reduction over $\text{KCaSrTa}_5\text{O}_{15}$ nanorod prepared by a polymerized complex method, *Bull. Chem. Soc. Jpn.* 88 (2015) 538–543.
- [24] P. Wang, L. Schwertmann, R. Marschall, M. Wark, Tetragonal tungsten bronze-type nanorod photocatalysts with tunnel structures: Ta substitution for Nb and overall water splitting, *J. Mater. Chem. A* 2 (2014) 8815–8822.
- [25] X. Liu, N. Fechner, M. Antonietti, Salt melt synthesis of ceramics, semiconductors and carbon nanostructures, *Chem. Soc. Rev.* 42 (2013) 8237–8265.
- [26] Y. Mizuno, H. Wagata, K. Yubuta, N. Zettsu, S. Oishi, K. Teshima, Flux growth of $\text{Sr}_2\text{Ta}_2\text{O}_7$ crystals and subsequent nitridation to form SrTaO_2N crystals, *CrystEngComm* 15 (2013) 8133–8138.
- [27] M. Kakihana, K. Domen, The synthesis of photocatalysts using the polymerizable-complex method, *MRS Bull.* 25 (2000) 27–31.
- [28] M. Yoshino, M. Kakihana, W.S. Cho, H. Kato, A. Kudo, Polymerizable complex synthesis of pure $\text{Sr}_2\text{Nb}_x\text{Ta}_{2-x}\text{O}_7$ solid solutions with high photocatalytic activities for water decomposition into H_2 and O_2 , *Chem. Mater.* 14 (2002) 3369–3376.
- [29] Y. Miseki, H. Kato, A. Kudo, Water splitting into H_2 and O_2 over $\text{Ba}_5\text{Nb}_4\text{O}_{15}$ photocatalysts with layered perovskite structure prepared by polymerizable complex method, *Chem. Lett.* 35 (2006) 1052–1053.
- [30] K. Sayama, H. Arakawa, Effect of carbonate addition on the photocatalytic decomposition of liquid water over a ZrO_2 catalyst, *J. Photochem. Photobiol. A: Chem.* 94 (1996) 67–76.
- [31] J. Liang, Y. Cao, H. Lin, Z. Zhang, C. Huang, X. Wang, A template-free solution route for the synthesis of well-formed one-dimensional Zn_2GeO_4 nanocrystals and its photocatalytic behavior, *Inorg. Chem.* 52 (2013) 6916–6922.
- [32] J. Boltersdorf, N. King, P.A. Maggard, Flux-mediated crystal growth of metal oxides: synthetic tunability of particle morphologies, sizes, and surface features for photocatalysis research, *CrystEngComm* 17 (2015) 2225–2241.
- [33] M. Hojamberdiev, K. Yubuta, J.J.M. Vequizo, A. Yamakata, S. Oishi, K. Domen, K. Teshima, NH_3 -assisted flux growth of cube-like BaTaO_2N submicron crystals in a completely ionized nonaqueous high-temperature solution and their water splitting activity, *Cryst. Growth Des.* 15 (2015) 4663–4671.
- [34] X. Li, J.J. Lenhart, Aggregation and dissolution of silver nanoparticles in natural surface water, *Environ. Sci. Technol.* 46 (2012) 5378–5386.
- [35] A.M. Ferraria, A.P. Carapeto, A.M.B. do Rego, X-ray photoelectron spectroscopy: silver salts revisited, *Vacuum* 86 (2012) 1988–1991.
- [36] S. Gao, Z. Li, K. Jiang, H. Zeng, L. Li, X. Fang, X. Jia, Y. Chen, Biomolecule-assisted in situ route toward 3D superhydrophilic Ag/CuO micro/nanostructures with excellent artificial sunlight self-cleaning performance, *J. Mater. Chem.* 21 (2011) 7281–7288.